Astron. Astrophys. 340, 241–256 (1998)

ASTRONOMY AND ASTROPHYSICS

Non-equilibrium chemistry in the dissipative structures of interstellar turbulence

K.Joulain[1], **E.Falgarone**[1], **G.Pineau des Forêts**[2], **and D.Flower**[3]

[1] Radioastronomie, CNRS, URA 336, Ecole Normale Supérieure, 24 rue Lhomond, F-75005 Paris, France
[2] D.A.E.C, CNRS, URA 173, Observatoire de Paris, F-92195 Meudon Principal Cedex, France
[3] Physics Department, The University, Durham DH1 3LE, UK

Received 5 May 1998 / Accepted 16 September 1998

Abstract. We study the chemical evolution of low density gas trapped in a vortex, representative of the dissipative structures of turbulence in the diffuse medium. A magnetic field is present and is close to being aligned locally with the vorticity. The chemical evolution is concentrated within tiny regions ($\approx$ 10 AU) and short timescales ($\lesssim$ a few 100 yr). It is controlled by the sharp temperature rise following the passage through layers where viscous dissipation is intense, and by the ion–neutral drift in layers where the tangential velocity of the neutrals is large. The facts that these two processes are closely associated in space and time, and that the amount of energy available in the dissipative structures is large, could explain, without fine-tuning the parameters of the model, the salient features of the observations of molecular species in diffuse gas: the large column densities of CH^+, OH and HCO^+, the remarkable proportionality of the OH and HCO^+ column densities, the similarity of the OH and HCO^+ (resp. CH and CH^+) line centroids, and the fact that the OH-rich gas seen in absorption is not always detected in emission. A large number of such vortices must be intercepted at any time on any line of sight to reproduce the observed column densities but we show that less than one percent of the gas column density need to be in those chemically active regions. The turbulent energy dissipated in all these structures is, on average, smaller than that available in the turbulent cascade of the diffuse medium. Last, the dependence of our results on the gas density confirms that this 'hot' chemistry must arise in low density gas in order to meet the requirements of the observations.

Key words: ISM: evolution – ISM: kinematics and dynamics – ISM: molecules – turbulence

1. Introduction

Diffuse interstellar clouds appear more chemically active than anticipated, given their low gas density and temperature. In particular, the large observed abundances of CH^+ and OH imply formation routes for these molecules which require energy sources much in excess of the average energy density of diffuse clouds. The formation of CH^+ proceeds through the endothermic reaction $C^+ + H_2 \rightarrow CH^+ + H$ with $\Delta E/k$ = 4640 K, and the formation of OH via O + $H_2 \rightarrow$ H + OH, which has an activation energy ($\Delta E/k$ = 2980 K); the main other formation route, induced by cosmic ray ionization, is unable to reproduce the large abundances observed in absorption in the radio domain.

In a previous work, we explored the impact of turbulence and its property of intermittency upon the chemistry of interstellar clouds. The intermittent nature of incompressible turbulence was first predicted theoretically by Landau and Lifshitz (1959), who postulated that the viscous dissipation of the turbulent kinetic energy was not uniform in space and time but occurred in bursts, with the subset of space in which these bursts occur filling only a tiny fraction of the available volume. We argued that the assumption of incompressibility is supported by the results obtained by Porter, Pouquet & Woodward (1994) in their simulations of compressible turbulence. They showed that shocks form very early, that they interact with one another and generate vorticity. After only one turnover time of the integral scale, most of the power in the high frequency modes is contained in the solenoidal (incompressible) modes and the small scale dissipation is therefore not dominated by that occurring in shocks but by viscous dissipation in the regions of large vorticity (or shear). We proposed that regions heated by violent bursts of dissipation of turbulent kinetic energy become chemically active within cold clouds. The local heating rate due to viscous dissipation was estimated in regions of large shear of the velocity field (Falgarone & Puget 1995, herafter FP). This heating rate depends on the strength of the intermittent event (i.e. the amplitude of the shear) and in most diffuse clouds, it locally exceeds all the other heating rates (due to cosmic rays or UV photons). We then investigated the chemical signatures of these warm regions in otherwise cold clouds (Falgarone, Pineau des Forêts & Roueff 1995, herafter FPR): the large local elevation of temperature triggers endothermic reactions and reactions with activation energies. We were able to successfully reproduce the column densities of CH^+ observed in diffuse clouds using dissipation rates for the turbulence consistent with cloud energy balance.

Nonetheless, our model, like most of those which have been proposed to explain the unexpected chemical activity of diffuse

Send offprint requests to: E. Falgarone

clouds (see for instance Federman et al. 1996a), has its limitations. It produces column densities of OH which are larger than those observed. A possible explanation relates to the extrapolation, to the low density of interstellar gas, of the temperature dependence of reaction rate coefficients; these are generally measured in conditions where all modes of the reactants are thermalized, a situation which does not obtain at lower density. On the other hand, models of magneto-hydrodynamical (MHD) shocks (Draine 1980; Pineau des Forêts et al. 1986), in which the gas kinetic temperature of the neutrals never reaches as large a value as in the intermittent turbulence model, are able to reproduce the observed column densities of OH, CH^+ and HCO^+ only when the shock velocity approaches 10 km s^{-1}. Whether the observed width and line centroid distributions of the CH and CH^+ lines (Crane et al. 1995, Crawford 1995, Gredel 1997) or OH and HCO^+ lines (Lucas & Liszt 1994, 1996; Liszt & Lucas 1996) are compatible with MHD shock models remains to be established (Flower & Pineau des Forêts 1998).

In the present paper, we explore further the chemical processes which may take place in the dissipative structures of turbulence, by introducing effects linked to the existence of a magnetic field, to which the neutrals are not directly coupled. In Sect. 2, we describe the model of a vortex which we adopt for the description of the dissipative structures and the morphology of the magnetic field. The kinematic and magnetic structures are assumed to be in steady-state, whereas the chemical and thermal processes are time-dependent. In Sect. 3, we describe the time-dependent thermal and chemical evolution of the gas and present the dependence of the results on a few important parameters. In Sect. 4, we compare these results with the relevant observations. We then describe the energy balance including all the scales involved (Sect. 5). In Sect. 6, we discuss the validity of the steady-state assumption of the hydrodynamic and magnetic structure and propose an alternative scenario which takes into account the large thermal and chemical inertia of the gas.

2. A template for the dissipative structures: the Burgers vortex

2.1. The vorticity structure

The intermittent property of turbulence manifests itself in the non–Gaussian distribution of vorticity and velocity increments observed in the laboratory or atmospheric flows of large Reynolds number (Anselmet et al. 1984; Tabeling et al. 1996). This statistical property may be related to the formation of coherent vortex structures in turbulent flows at high Reynolds number. A comparison of numerical simulations of flows at high Reynolds numbers, either incompressible (She, Jackson & Orszag 1990; Vincent & Meneguzzi 1991, 1994) or compressible (Porter, Pouquet & Woodward 1992; 1994) leads to the unexpected result that the properties of the regions of intense vorticity in both the compressible and incompressible cases are very similar. But laboratory experiments such as those of Douady, Couder & Brachet (1991), Cadot et al. (1995) and Belin et al. (1996) are the only means of investigation of the characteristics of these vortices because numerical simulations cannot properly describe scales close to the dissipation scale. These recent experiments show that these vortices have a cross-sectional radius somewhere between the inner Kolmogorov scale (or the dissipation scale) and the Taylor microscale and lengths as large as the integral scale (the scale on which the turbulent energy is injected). The lifetime of the largest vortices is observed to be of the order of the turn-over timescale of the integral scale, i.e. up to about 100 times, or more, the vortex period. That of the smallest vortices, of size close to the dissipation scale, may not exceed a few periods. Another property of these vortices is their crowding. Experiments (Schwarz 1990) and numerical simulations (Porter et al. 1994; Vincent & Meneguzzi 1994) show that structures of intense vorticity in turbulence are not isolated and randomly distributed in space but bunched together in both space and time, because they seem to result from instabilities which develop in a larger scale shear layer.

Considering the above, we chose to model the dissipative structures by the Burgers vortex, an exact solution of the Helmholtz equation for the evolution of vorticity in an incompressible fluid. This solution allows an analytical description of the velocity field in the regions of interest for the chemistry. It connects the vorticity structure to the properties of the straining large scale flow (see Moffatt, Kida & Ohkitani 1994). We adopt an axisymmetric irrotational straining flow, characterized in (r, θ, z) cylindrical coordinates by $u_r(r) = -a\,r\,/\,2$ and $u_z(z) = a\,z$ where a is the strain coefficient. The vorticity distribution, axisymmetric in this case,

$$\omega(r) = \omega_0 \mathrm{e}^{-\frac{r^2}{r_0^2}}, \tag{1}$$

corresponds to an equilibrium between the stretching of the vortex by the turbulent strain a, which tends to increase the vorticity, and the diffusion of vorticity. The equilibrium vortex radius r_0 therefore depends only on the turbulent strain rate a and the kinematic viscosity ν, through the relation:

$$r_0^2 = \frac{4\nu}{a}. \tag{2}$$

The peak of vorticity, ω_0 is related to the vortex circulation $C = \int_0^\infty \omega(r) 2\pi r dr$ by $\omega_0 = aC/4\pi\nu$.

Any Burgers vortex is therefore entirely described by two parameters, ω_0 and r_0, related to the two independent parameters C, the circulation of its vorticity and a the strain rate exerted by its environment. The tangential velocity is also axisymmetric,

$$u_\theta(r) = \frac{\omega_0 r_0^2}{2r}(1 - \mathrm{e}^{-\frac{r^2}{r_0^2}}), \tag{3}$$

and so too is the viscous dissipation rate, defined as

$$\Gamma_d = \frac{\eta}{2} \sum_{i,j} \left(\frac{\partial u_i}{\partial x_j} + \frac{\partial u_j}{\partial x_i} \right)^2 \tag{4}$$

where $\eta = \rho\nu$ is the dynamic viscosity in a gas of density ρ. In cylindrical symmetry, the dominant contribution to the viscous dissipation is:

$$\Gamma_d(r) \;=\; \eta \left(\frac{\partial u_\theta}{\partial r} - \frac{u_\theta}{r} \right)^2 \tag{5}$$

$$= \eta\omega_0^2 \left[e^{-\frac{r^2}{r_0^2}} \left(1 + \frac{r_0^2}{r^2}\right) - \frac{r_0^2}{r^2} \right]^2 . \quad (6)$$

This model is highly idealized but, as will be seen below, it allows us to introduce all the ingredients we need, with a modest number of free parameters, and to test quantitatively for the first time the combined effects of viscous dissipation and ion-neutral drift within a single dissipative structure.

We now estimate the parameters r_0 and ω_0 of those of the Burgers vortices which are able to locally trigger 'hot' chemistry in a cloud of average density $n_{\rm H} = 30\,{\rm cm}^{-3}$ and low temperature $T_{\rm k} \approx 100$ K. One derives from Eqs. (3) and (6) that in the Burgers vortex, the tangential velocity and the viscous dissipation rate have maxima $u_{\theta,max} = 0.3\,\omega_0\,r_0$ and $\Gamma_{d,max} = 0.09\,\eta\,\omega_0^2$. Therefore, any set of parameters $(\omega_0,\, r_0)$ determines $\Gamma_{d,max}$ and $u_{\theta,max}$.

The first constraint regards the viscous heating rate. Following FP and FPR, the vortices generate chemically active regions if the local heating rate due to viscous dissipation Γ_d exceeds about $10^{-22}\,{\rm erg\,cm^{-3}s^{-1}}$. The second constraint regards $u_{\theta,max}$. It is related to the fact that, in numerical simulations of incompressible turbulence at high Reynolds number (Jimenez 1997) and in flow experiments (Belin et al. 1996), the maximum tangential velocity of vortex filaments is found to be equal to the rms velocity dispersion of the large scale turbulence. The internal velocity dispersion of clouds seen in H I emission is observed to range between 2.9 and 3.7 km s^{-1} (Crovisier 1981), and we therefore impose $u_\theta \lesssim 4$ km s^{-1}. The lower limit to the viscous heating rate turns into a lower limit to the central vorticity:

$$\omega_0 > 2.9 \times 10^{-9}\,{\rm s}^{-1}, \quad (7)$$

and the upper limit to the tangential velocity into an upper limit to the vortex radius:

$$r_0 < 3.8 \times 10^{14}\,{\rm cm} = 25\,{\rm AU}. \quad (8)$$

We have adopted a dynamic viscosity $\eta = 6 \times 10^{-6}$ g cm^{-1} s$^{-1} T_{\rm k}^{1/2}$ (Kay & Laby 1966) and the kinematic viscosity is therefore $\nu = 8.5 \times 10^{17}$ cm^2 s$^{-1} (T_{\rm k}/100\,{\rm K})^{1/2} (n_{\rm H}/30\ {\rm cm}^{-3})^{-1}$.

It is interesting to compare the vortex radius to the dissipation length of turbulence and to the particle mean free path. The dissipation length is estimated to be $l_d = (\nu^3/\epsilon)^{1/4}$ in a turbulent cascade, where ϵ is the transfer rate of specific kinetic energy. In FP, this rate was estimated to range between $\epsilon = 10^{-3}$ and 0.2 erg g^{-1} s^{-1} in diffuse clouds, so that $l_d = 8.8 \times 10^{13}{\rm cm} = 5.9\left(\epsilon/0.01\,{\rm erg\,g^{-1}\,s^{-1}}\right)^{-0.25}$ AU. The mean free path of H atoms, for H–H elastic collisions of cross section $\sigma_c = 5.7 \times 10^{-15}$ cm^2, is $\lambda = 5.8 \times 10^{12}$ cm = 0.39 AU. The vortex radius which is at least of the order of the dissipation length is therefore more than 15 times larger than the H mean free path, which justifies the hydrodynamical approach adopted here to describe the dissipative structures of the medium.

The vortex period is $P \lesssim 2\pi/\omega_{0,min} = 2.2 \times 10^9$ s = 72 yr and the time spent to spiral inward between the distances r_1 and $r_2 < r_1$ from the vortex axis (i.e. crossing time) is:

$$\tau_c = \frac{2}{a} \ln(\frac{r_1}{r_2}). \quad (9)$$

2.2. The magnetic field configuration

Numerical simulations of three–dimensional MHD turbulence over a significant dynamical range are rare. Relevant to the dynamics of the interstellar medium, the case of two fluids (ionized and neutral) weakly coupled by collisions has never been treated. Yet, recent simulations of turbulent dynamo (Brandenburg et al. 1996) seem to confirm the similarity between the dynamics of magnetic field and vorticity, anticipated in view of the similarities of the equations which describe their evolution (e.g. Brandenburg, Procaccia and Segel 1995). In addition to the intermittent distribution in space of the magnetic field intensity already found by Meneguzzi & Pouquet (1981) (i.e. like vorticity, the magnetic field is concentrated in regions which fill only a small fraction of the volume), Brandenburg et al. show that the magnetic field and the vorticity vectors tend to align with each other, being parallel or anti-parallel. Although these simulations refer to a medium fully coupled to the magnetic field, it is possible that the same configuration be found in a gas only weakly coupled to the field, for the following reasons. As discussed by Bajer (1995), the field lines of a component perpendicular to the vortex axis would tend to wind in a double spiral with the direction of the field alternating in the spiral. Ambipolar diffusion would then form sharp structures around magnetic nulls, at scales possibly small enough for reconnection to occur, thus annihilating the field component perpendicular to the vortex axis (Brandenburg & Zweibel, 1994). Although this scenario clearly deserves further work, we have adopted a geometry where the magnetic field and the vorticity are parallel for the *initial* conditions in the computation described below, because it is a probable configuration.

In the problem that we address here, there are a few timescales of importance. The timescale for momentum transfer of an ion (e.g. C^+) in a sea of neutrals (mainly H and H_2) is $\tau_{in} \approx (\mu_n + \mu_i)/(\mu_n n_n \langle\sigma v\rangle_{in})$, where μ_i and μ_n are the mean mass per particle in the ions and neutrals respectively, n_n is the neutral number density and $\langle\sigma v\rangle_{ni} = 2 \times 10^{-9}$ cm^3 s^{-1} is the momentum transfer rate coefficient (Flower & Pineau des Forêts 1995). For $n_n = 30$ cm^{-3}, $\tau_{in} \approx 2 \times 10^8$ s. This is much larger than the ion cyclotron period of approximately 10^4 s for B ≈ 10 μG. Accordingly, the magnetic field lines may be considered to be frozen in the ions, whose motion decouples significantly from that of the neutrals (i.e. ion-neutral drift occurs).

We have computed the time–dependent evolution of the ion velocity $\mathbf{v}_i$ and magnetic field configuration $\mathbf{B}(r,\theta,z)$ for a fluid initially at rest and pervaded by a uniform magnetic field $\mathbf{B}(0,0,B_z)$ which is perturbed by a Burgers vortex generated

in the fluid of neutrals at $t = 0$. The equation of motion of the ions (neglecting the pressure gradients):

$$\rho_i(\frac{\partial \mathbf{v}_i}{\partial t}+(\mathbf{v}_i.\boldsymbol{\nabla})\mathbf{v}_i) = -\gamma\rho_n\rho_i(\mathbf{v}_i-\mathbf{v}_n)+\frac{1}{4\pi}(\boldsymbol{\nabla}\times\mathbf{B})\times\mathbf{B} \quad (10)$$

where $\gamma = \langle\sigma v\rangle_{in}/(\mu_i+\mu_n) \approx 10^{14}$ cm^3 s^{-1} g^{-1} for C^+-H collisions, and the equation of evolution of the magnetic field:

$$\frac{\partial \mathbf{B}}{\partial t} = \boldsymbol{\nabla}\times(\mathbf{v}_i\times\mathbf{B}) \quad (11)$$

reduce to their projections in the tangential direction because the motions of the neutrals in the r and z directions, which determine the confinement and stretching of the vortex, do not enter explicitly into the equation of motion in the θ direction. The tangential projection of the equation of motion is:

$$\rho_i\left(\frac{\partial v_{i\theta}}{\partial t}+v_{ir}\frac{\partial v_{i\theta}}{\partial r}+v_{ir}\frac{\partial v_{i\theta}}{\partial z}+\frac{v_{ir}v_{i\theta}}{r}\right) =$$

$$-\gamma\rho_n\rho_i(v_{i\theta}-v_{n\theta})+\frac{1}{4\pi}\left(B_z\frac{\partial B_\theta}{\partial z}+\frac{B_rB_\theta}{r}+B_r\frac{\partial B_\theta}{\partial r}\right) \quad (12)$$

and the equation of evolution of B_θ is:

$$\frac{\partial B_\theta}{\partial t} = B_r\frac{\partial v_{i\theta}}{\partial r}+\frac{v_{ir}B_\theta}{r}+B_z\frac{\partial v_{i\theta}}{\partial z}$$

$$-v_{ir}\frac{\partial B_\theta}{\partial r}-\frac{v_{i\theta}B_r}{r}-v_{iz}\frac{\partial B_\theta}{\partial z} \quad (13)$$

In the above equations, the neutral tangential velocity $v_{n\theta} = u_\theta$, given by Eq. (3), is considered to be independent of time during the lifetime of the vortex, and $v_{i\theta}$ is the ion velocity, which differs from the neutral velocity owing to their decoupling. In what follows, we use the ion-neutral drift velocity defined as $v_D = v_{n\theta} - v_{i\theta}$.

We are interested in the existence of steady–state solutions in which the ions keep a significant drift velocity relative to the neutrals. If the neutral rotation velocity is independent of z, the ions couple to the neutrals on the timescale for momentum transfer, τ_{in}. However, the vorticity filaments have a finite length L, and so $v_{n\theta}$ varies along the vortex axis. This finite length therefore defines the boundary conditions for $v_{n\theta}$ i.e. $v_{n\theta} = u_{\theta,max}$ at $z = 0$ and $v_{n\theta} = 0$ at $z = \pm L/2$.

Even a small dependence of $v_{n\theta}$ on z introduces a dependence of $v_{i\theta}$ on z which in turn generates a B_θ component of the magnetic field. It is the variation of the tangential component of the magnetic field along the z axis which allows the Lorentz force to balance that due to ion–neutral momentum transfer. We find that the timescale for reaching the steady–state configuration is as short as the filament length is short and the B_z component is large. For $B_z = 10\mu$G and a linear decrease of $v_{n\theta}$ from its maximum value, given by Eq. (3), at $z = 0$ to $v_{n\theta} = 0$ at $z = 1.5\times10^{15}$ cm (vortex length = 3×10^{15} cm $\approx$ 200 AU), steady–state with $v_{i\theta} \lesssim 0.1$ km s^{-1} is reached at $t = 8\times10^8$ s. In this steady-state, B_θ decreases almost linearly with z from $B_\theta = 0$ μG at $z = 0$ to $B_\theta = 0.1$ μG at the ends of the vortex.

3. The thermal and chemical evolution of the gas trapped in a vortex

3.1. Description of the model

We follow the time-dependent thermal and chemical evolution of a fluid particle which enters the vortex. The initial conditions are the kinetic temperature, density and equilibrium chemical composition characteristic of diffuse clouds. The flow is the steady-state configuration of the Burgers vortex: the particle velocity is not derived from the usual laws of conservation of momentum and energy. Note that the solutions of the Helmholtz equation satisfy all equations of motion in which the radial forces derive from a potential with cylindrical symmetry. The corresponding source of energy is ignored here, owing to the fact that an analytical description of the large scales (i.e. the straining flow) is beyond the scope of the present study and irrelevant to the points we wish to stress. The energy balance is discussed from a global point of view in Sect. 5.

The evolution of the fluid particle is followed in a comoving reference frame. Three fluids are considered: the neutrals, the ions and the electrons. The chemical evolution, the density and the temperature of each of the three fluids are calculated simultaneously by means of the GEAR differential equation solver. The neutral flow velocity is generated by numerically solving differential equations which correspond to the imposed velocity profile. This procedure ensures that the time step is consistent with slow variations of all the significant dependent variables. The ionized particles are assumed to be bound to the magnetic field lines. Herafter are the equations that we integrate along the fluid particle trajectory.

Although the fluid particle is assumed to be incompressible, the mass densities of the neutrals and the ions can change through chemical reactions. The chemical network is an updated and reduced version of that used by Le Bourlot et al. (1993). It includes 41 chemical species and 278 chemical reactions. Gas phase abundances of carbon and oxygen are depleted relative to the Solar values of Anders & Grevesse (1989) by $\delta_C = 0.4$ and $\delta_O = 0.8$ so that [C]/[H]=1.4×10^{-4} and [O]/[H]=6.7×10^{-4}. Following Flower et al. (1985), we introduce an effective temperature for reactions involving an ion and a neutral which includes the miscroscopic (different kinetic temperatures) and macroscopic (ion-neutral drift velocity) relative kinetic energies of the ionized and neutral particles. Keeping the notations of Flower et al. (1985), we denote by $\mathcal{C}_\alpha$ the rate at which species α is produced per unit volume and time, and by m_α its mass. The source term for the mass of each species is therefore:

$$S_k = \sum_\alpha \mathcal{C}_\alpha m_\alpha \quad \text{for } k = n, i. \quad (14)$$

The evolution of the mass densities of the neutral and the ionized fluids is given by:

$$\frac{d\rho_k}{dt} = S_k \quad \text{for } k = n, i. \quad (15)$$

As the mass of the fluid cell is conserved in the chemical reactions, $S_i = -S_n$. Similarly, the variations of the number densities of the neutral and ionized fluids are given by:

$$\frac{dn_k}{dt} = Y_k \tag{16}$$

where $Y_k = \sum_\alpha \mathcal{C}_\alpha$.

The time dependence of the thermal energy density, $U = \frac{3}{2} n_n k T_n$, where T_n is the neutral temperature, is determined by

$$\frac{dU}{dt} = B_n + \Gamma_d, \tag{17}$$

where Γ_d is the viscous dissipation rate defined in Eq. (4). Note that it is independent of the particle mean free path and depends only on the characteristics of the velocity field, on the mean mass per particle and the temperature. B_n is a sum of heating and cooling terms which are described by Flower et al. (1985). In particular, the contributions to the heating of ion–neutral and electron–neutral scattering are

$$B_n^{(in)} = \frac{\rho_n \rho_i}{\mu_n \mu_i} \langle \sigma v \rangle_{in} \frac{2\mu_n \mu_i}{(\mu_n + \mu_i)^2}$$

$$\left[\frac{3}{2} k (T_i - T_n) + \frac{1}{2} \mu_i (\boldsymbol{u}_i - \boldsymbol{u}_n)^2 \right] \tag{18}$$

and

$$B_n^{(en)} = \frac{\rho_n \rho_i}{\mu_n \mu_i} \langle \sigma v \rangle_{en} \frac{2\mu_e}{\mu_n}$$

$$\left[\frac{4}{2} k (T_e - T_n) + \frac{1}{2} \mu_e (\boldsymbol{u}_i - \boldsymbol{u}_n)^2 \right]. \tag{19}$$

In these expressions T_i and T_e are the ion and electron temperatures, and μ_i and μ_e are the mean molecular weights of the ions and electrons, respectively. The time derivative of T_n is:

$$\frac{dT_n}{dt} = \frac{2}{3 k n_n} \left(B_n + \Gamma_d - \frac{3}{2} k T_n \frac{dn_n}{dt} \right). \tag{20}$$

In our model, the values of the ion and the electron temperatures are assumed to be equal, and governed by:

$$\frac{dT_e}{dt} = \frac{dT_i}{dt} = \frac{2}{3 k n_i} \left(B_i + B_e - \frac{3}{2} k T_i \frac{dn_i}{dt} \right). \tag{21}$$

where B_i and B_e are the sums of heating and cooling terms for the ions and the electrons, respectively. The terms B_n and B_e include the radiative losses due the collisional excitation of the fine structure levels of C^+, C and O, of the ro-vibrational levels of H_2 and of the rotational levels of H_2O, OH and CO (Flower, Pineau des Forêts & Hartquist 1986). Together with the equations which determine the chemical evolution of the fluids, there is a total of 53 first-order differential equations to solve. Integrating these equations yields the chemical composition and the physical properties of the fluids at any point in the vortex. In practice, the flow variables depend only on the distance from the vortex axis, r which decreases exponentially with time.

3.2. The standard model

The radial dependence of the vorticity, ion-neutral drift velocity, viscous heating rate and neutral gas kinetic temperature are displayed in Fig. 1, for what will be referred to as the standard model. This model is characterized by four independent parameters: two parameters which describe the vortex, i.e. $\Gamma_{d,max} = 10^{-21}$ erg cm^{-3}s^{-1} and $u_{\theta,max} = 3.5$ km s^{-1} or, equivalently, $\omega_0 = 9.2 \times 10^{-9}\,\mathrm{s}^{-1}$ and $r_0 = 1.2 \times 10^{14}$ cm = 8 AU, and two parameters which characterize the ambient medium, i.e. the total cloud density $n_\mathrm{H} = 30\,\mathrm{cm}^{-3}$ and the shielding of the dissipative structure from the interstellar radiation field (ISRF), $A_{v0} = 0.2$ mag, both typical of diffuse clouds. This shielding is due to the medium surrounding the vortex and is not directly related to the mean extinction A_v toward a star, although one would expect $A_v \gtrsim A_{v0}$. The selected value of the turbulent heating term at its maximum characterizes those bursts which are neither the most powerful (the rarest) nor the weakest (the most numerous) which would not significantly affect the chemistry (see Table 1 of FPR). The maximum tangential velocity is close to the Alfvén velocity in the neutral fluid $v_A = 3.6$ km s^{-1} $(B/10\mu\mathrm{G})\left(n_\mathrm{H}/30\,\mathrm{cm}^{-3}\right)^{1/2}$. The adopted magnetic field intensity is inferred from Zeeman effect measurements in the 21 cm HI line in diffuse clouds (Myers et al. 1995). The corresponding straining rate is $a = 5.3 \times 10^{-10}$ s^{-1}; this value derives from Eq. (2), using the kinematic viscosity computed at $T_\mathrm{k} = 500$ K, the gas temperature at $r = 1.2\,r_0$ where the Laplacian of the vorticity, and therefore the diffusion, has its maximum (see Fig. 1).

The layers in which the ion-neutral drift $v_D = |v_n - v_i|$ exceeds 3 km s^{-1} and the kinetic temperature T_n exceeds 10^3 K are indicated in Fig. 1. The comparison of panels (b) and (d) shows that the layers in which the chemistry is dominated by ion-neutral drift are not identical to those in which it is dominated by thermal effects. In the standard model, the time spent by a fluid particle in the layers where $v_D > 3$ km s^{-1} is therefore, according to Eq. (9), $\tau = 127$ yr and that spent in the layers where $T_n > 10^3$ K is $\tau = 190$ yr.

This figure also shows that the peak kinetic temperature is reached at a smaller distance from the vortex axis ($r = 6 \times 10^{13}$cm) than that ($r = 1.2 \times 10^{14}$cm) at which the maximum viscous dissipation occurs. The thermal inertia of the medium is such that ≈ 100 yr are needed for the gas to reach a temperature maximum after having experienced a heating burst. In addition and for the same reason, the duration of the heating burst, defined as the time during which $\Gamma_d > 5 \times 10^{-22}$ erg cm^{-3}s^{-1}, is $\tau \approx 100$ yr, about half the time during which the fluid cell temperature is raised above 10^3 K. It should also be noted from Fig. 1d (since $\partial T/\partial t = -(ar/2)\,\partial T/\partial r$) that the gas trapped in the vortex almost never reaches a steady-state temperature: it is always either being heated or cooling. This is an important characteristic of the model, as will be seen later. Departures from thermal and chemical equilibrium increase with the inward radial velocity u_{nr} of the neutral fluid.

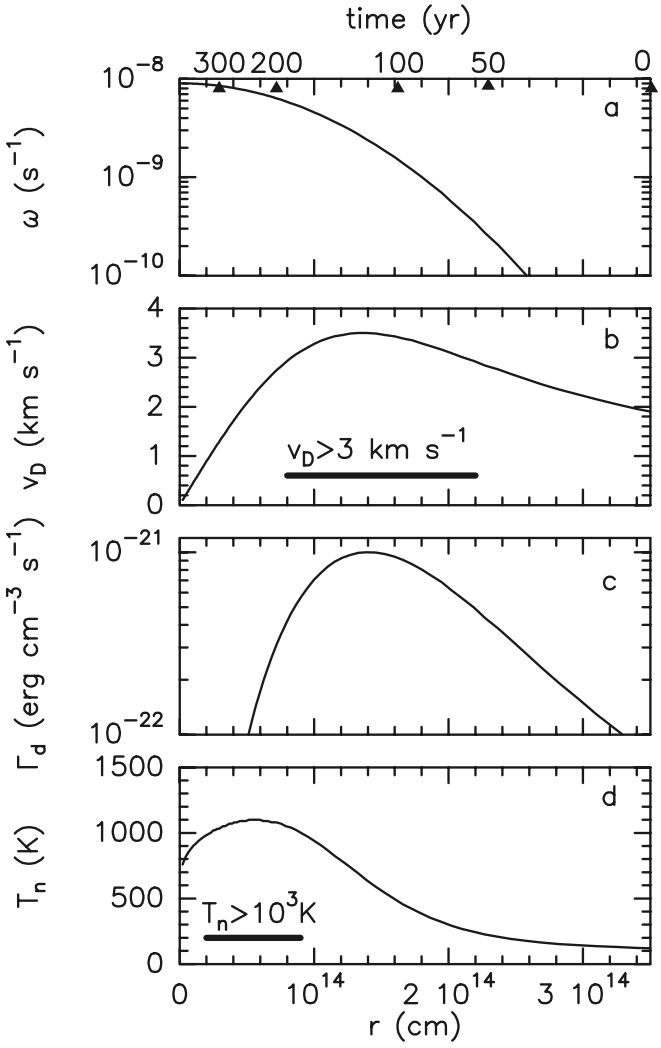

Fig. 1a–d. The radial dependence of (**a**) the vorticity ω, (**b**) the ion–neutral drift velocity v_D, (**c**) the heating rate due to the viscous dissipation Γ_d, and (**d**) the neutral gas kinetic temperature T_n. The horizontal bars delineate the layers where $v_D > 3$ km s^{-1} and $T_n > 10^3$ K i.e. where the 'hot' chemistry is active. Note that the radial dependence also implies a time dependence, according to Eq. (9). The corresponding time scale is shown on the upper axis.

3.3. Results

Before studying the influence of the model parameters upon the results, we first present the chemical evolution of a fluid particle in the case of the standard model. This model, as said before, corresponds to the structures which are the most likely to affect the chemistry, while staying consistent with observational constraints on the vortex parameters. Dissipative bursts exist everywhere and vortices are likely to appear also in pure atomic gas, weakly shielded from the ambient UV field. In such a case, the lifetime of newly formed molecules is likely to be small owing to the rapidity of the photodissociation process. For the shielding ($A_{v0} = 0.2$ mag) and gas density of the standard model, and the H_2 photodissociation rates computed by Abgrall et al. (1992), one finds $n(H_2) = 13.4$ cm^{-3} and $n(H) = 3.2\,\mathrm{cm}^{-3}$. This $[H_2]/[H]$ ratio is larger than the *average* values determined from observations in absorption against stars (Savage et al. 1977). However, the *local* $[H_2]/[H]$ abundance ratio is likely to be unevenly distributed along the line of sight and inadequately traced by the measured average value. In the present work we compute the chemical enrichment provided to the medium by those vortices which form in moderately shielded pockets of gas along a line of sight.

The evolution of the fractional abundances of a subset of chemical species are shown in Fig. 2 as a function of r, the distance to the vortex axis, or equivalently of time according to Eq. (9). The initial abundances are equilibrium abundances obtained for $n_{\mathrm{H}} = 30\,\mathrm{cm}^{-3}$. As the fluid particle approaches the vortex axis the dominant reaction schemes responsible for the formation of a molecular species evolve. The reaction rates of endothermic reactions for instance increase by several orders of magnitude and most of the species have a fractional abundance which increases sharply as the fluid cell enters the vortex structure.

In the ambient medium, the OH production is dominated by the recombination of H_2O^+ and H_3O^+ with electrons. The chain of reactions producing these ions is initiated by the ionization of hydrogen by cosmic rays followed by charge transfer to oxygen, $H^+ + O \rightarrow H + O^+$, and subsequent hydrogenation reactions. This formation scheme is no longer dominant in the hot layers of the vortex where the activation barrier of the reaction $O + H_2$ can be overcome. The rate of OH formation via this reaction becomes more than one order of magnitude larger than all the others within the vortex. As expected, the OH fractional abundance (Fig. 2a) peaks in the region where the gas temperature attains a maximum. The abundance of H_2O which forms mainly via $OH + H_2 \rightarrow H_2O + H$ follows closely that of OH.

The endothermic reaction of C^+ with H_2 becomes important when the ion-neutral drift speed exceeds 3 km s^{-1}. It is followed by $CH^+ + H_2 \rightarrow CH_2^+ + H$ and $CH_2^+ + H_2 \rightarrow CH_3^+ + H$. This chain of reactions terminates with the formation of CH_3^+, which recombines with electrons faster than it reacts with H_2, producing CH. In the ambient gas, the only routes to initiate this chain of reactions are the slow radiative associations of C^+ with H and H_2 which initiate the formation of CH and CH^+ there. In the vortex, the CH abundance decreases where the temperature peaks because its main destruction paths are $CH + H_2 \rightarrow CH_2 + H$ and $CH + H \rightarrow C + H_2$, which have activation barriers $\Delta E/k$ = 1760 K and 2200 K, respectively. The existence of the activation barrier in the second of these reactions has been questioned (Harding, Guadagnini & Schatz 1993). If a temperature-independent rate constant $k_r = 5 \times 10^{-11}$ cm^3 s^{-1} is adopted, the CH fractional abundance increases by only 50%. A direct consequence of the destruction of CH in the hot layers is a rapid increase in the abundance of neutral carbon; in these layers, the fractional abundances of neutral and ionized carbon differ by no more than a factor ≈ 2. The C to C^+ abundance ratio in the vortex is therefore extremely different from its value ($\approx 10^{-3}$) in the ambient medium.

The abundances of most of the ions (Fig. 2b) follow the time history of the ion-neutral drift velocity. H_3O^+ is the only ion to

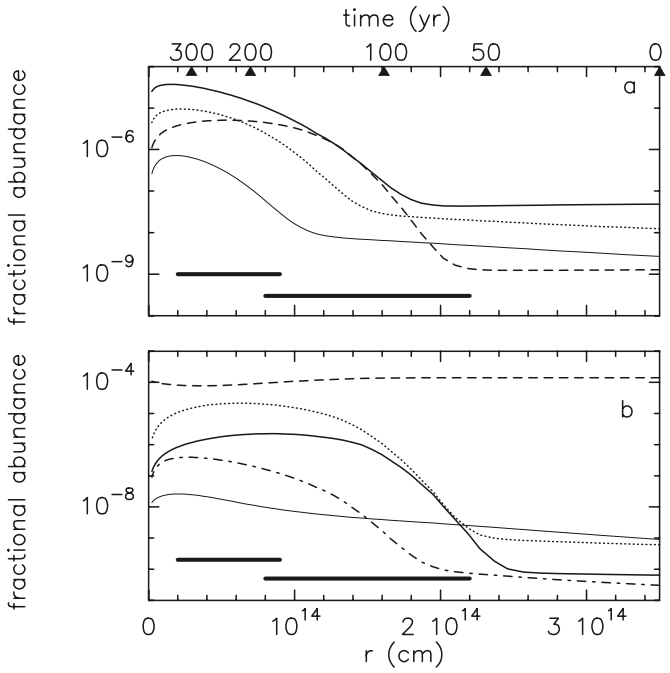

Fig. 2. a Fractional abundances of a set of neutral species, C (thick solid line), CH (dashed line), OH (dotted line), H_2O (thin solid line) as functions of the distance r of the fluid cell from the vortex axis. **b** Fractional abundances of a set of ions, C^+ (dashed line), CH^+ (thick solid line), CH_3^+ (dotted line), HCO^+ (dot-dashed line), H_3O^+ (thin solid line), as functions of r. The corresponding time scale is shown on the upper axis. The regions where the gas temperature exceeds 10^3 K and the ion-neutral drift velocity exceeds 3 km s^{-1} are delineated by the same horizontal bars as in Fig. 1.

differ because it forms in a series of reactions initiated by the charge transfer of H^+ with O; this reaction is endothermic by only 227 K and occurs even far from the vortex axis.

CH_3^+ is the most abundant ion after C^+ and can even become the most abundant ion in the layers with large ion-neutral drift. The formation of CH_3^+ terminates the chain of hydrogen abstraction reactions given above which commences with the reaction of C^+ with H_2 when the ion-drift speed exceeds about 3 km s^{-1}. The abundance of CH_3^+ increases more than CH^+ across the vortex because its formation rate stays larger than its destruction rate. A consequence of the large fractional abundance of CH_3^+ is that the formation of HCO^+ is dominated by

$$CH_3^+ + O \rightarrow HCO^+ + H_2$$

rather than by the reaction $C^+ + OH \rightarrow CO^+ + H$ followed by $CO^+ + H_2 \rightarrow HCO^+ + H$ which is the main route to form HCO^+ in the surrounding diffuse gas, the reaction of C^+ with H_2O being still less important. The abundance of CO (not shown) is enhanced by two orders of magnitude in the vortex. This enhancement is due to several reactions, mainly the dissociative recombination of HCO^+ but also the reactions of OH with C and C^+ and to a lesser extent of CO^+ with H.

The quantities of interest for comparison with observational data are the column densities of each species, integrated through all the dissipative structures intercepted by the line of sight and through the ambient medium. As seen before, these dissipative structures are tiny (radii $\approx$ 10 AU). At any time in a cloud, there is a large number of such vortices and a random line of sight across the cloud is expected to cross a subsample of these vortices. We will estimate in Sect. 4 that there are about one thousand vortices intercepted by a line of sight sampling 1 magnitude of gas. The observed column densities have therefore two origins: the large number of vortices intercepted by the line of sight and the ambient medium. These two contributions are given in Table 1 for a line of sight sampling $N_{\rm H} = N({\rm H}) + 2N({\rm H_2}) = 1.8 \times 10^{21}$ cm^{-2} (or 1 mag) with $n_H = 30$ cm^{-3}. To estimate the contribution from the ambient medium we have assumed that $N({\rm H_2})/N({\rm H}) = 1$. This fraction of molecular hydrogen is lower than in the vortices and corresponds to an upper limit of the values observed in the diffuse medium (Savage et al. 1997). For $N({\rm H_2})/N({\rm H}) = 0.17$, the molecular contributions from the ambient medium change by less than 20%, except those of CH and CO which decrease by a factor 3.5 and 2, respectively. N_v is the column density of each species integrated across one vortex. For comparison, the observed ranges of column densities for OH, CH^+, HCO^+, CH, CO and C are also given in Table 1. The observational techniques and samples are different for the various data sets and are discussed in Sect. 4. One should keep in mind that the total hydrogen column densities sampled by the observations in the visible range vary from 0.03 mag to 4.5 mag (or $N_{\rm H} = 5.4 \times 10^{19}$ to 8.1 $\times 10^{21}$ cm^{-2}).

3.4. Dependence of the results on the independent parameters of the model

Dissipative bursts of any strength may occur anywhere in a cloud, and it is essential to discuss the dependence of the results on the parameters which characterize a burst and the medium in which it occurs. The location of the burst in the cloud is determined by A_{v0}: close to the edge of a cloud, $A_{v0} < 0.1$ mag, whereas, in the more shielded regions, A_{v0} approaches 1. The local gas density has been varied over the range characteristic of diffuse clouds, $30\,{\rm cm^{-3}} < n_{\rm H} < 100\,{\rm cm^{-3}}$. The strength of the burst is described by two independent parameters, ω_0 and r_0 or equivalently, as shown in Sect. 2.1, the peak of the viscous heating rate $\Gamma_{d,max} \propto \omega_0^2$ and that of the tangential velocity of the neutrals, $u_{\theta,max} \propto \omega_0\, r_0$ which in turn determines the ion-neutral drift velocity v_D. The dissipation rate has been varied over the range considered by FPR as plausible in galactic clouds, 3×10^{-22} erg cm^{-3}s^{-1} $< \Gamma_{d,max} < 3\times10^{-21}$ erg cm^{-3}s^{-1}. The influence of the maximum tangential velocity, and therefore v_D, has been investigated for 3 km $s^{-1} < u_{\theta,max} <$4 km s^{-1}. Note that one parameter has been varied at a time, so that changing $\Gamma_{d,max}$ while keeping v_D constant, means changing ω_0 and r_0 accordingly. This modifies the crossing time $\tau_c \propto r_0^2$ (see Eqs. 2 and 9). Similarly, changing the density causes ν to vary, and, as the vortex parameters must be kept constant, a must be changed accordingly (see Eq. 2) and therefore τ_c. As will be seen below, the weak dependence of the results on most of the

Table 1. Column densities integrated across one thousand standard vortex filaments, across one magnitude in the ambient medium and ranges of observed values for line of sight extinctions ranging between 0.03 and 4.5 mag.

Species	Model	Ambient gas (1 mag)	Observations		Ref.
	$N_v \times 1000$	N_{amb}	N_{min}	N_{max}	
	(cm^{-2})	(cm^{-2})	(cm^{-2})	(cm^{-2})	
C	1.4×10^{14}	6.6×10^{13}	1×10^{13}	3×10^{15}	a
OH	3.5×10^{13}	2.1×10^{13}	8×10^{12}	2×10^{14}	b
			3×10^{13}	1×10^{14}	c,d,e
CH	3×10^{13}	1.3×10^{12}	2×10^{12}	7×10^{13}	f
			2×10^{12}	2.6×10^{13}	g
CO	2.9×10^{12}	7.2×10^{12}	1×10^{12}	$\approx 1 \times 10^{16}$	h,i
H_2O	2.1×10^{12}	2.9×10^{12}			
CH^+	1.5×10^{13}	1.1×10^{11}	3.5×10^{12}	7×10^{12}	j,k
			2×10^{12}	3.3×10^{13}	g
			3×10^{12}	8.5×10^{13}	f
CH_3^+	1.2×10^{14}	4.8×10^{11}			
HCO^+	1.6×10^{12}	4.5×10^{10}	3×10^{11}	8×10^{12}	b

a - Jenkins & Shaya (1979); b - Lucas & Liszt (1996); c - Felenbok & Roueff (1996); d - Federman et al. (1996b); e - Crutcher & Watson (1976); f - Gredel (1997); g - Crane et al. (1995); h - Federman et al. (1980); i - Data reported in Federman et al. (1994); j - Federman (1982); k - Reported in Meyer & Roth (1991).

parameters is due to the large thermal and chemical inertia of the gas.

The above parameters all act upon the amplitude of the temperature rise due to viscous dissipation and therefore upon the chemical evolution of the fluid. In addition to the importance of the timescales mentioned above, several processes compete with each other which mitigate the influence of the parameters and enhance the robustness of the results. The influence of A_{v0}, and therefore of the UV field, on the gas temperature is weak (the peak temperature T_{max} increases only by 20% over the explored range of A_{v0}) because of the two competing processes, both linked to the increase of the H_2 fraction with A_{v0}: the first is the increase in the rate of radiative cooling in the hot layers, due mainly to the ro-vibrational lines of H_2, the second is the decrease of the number of particles per unit volume as the hydrogen molecular fraction increases, which for a given input of energy per unit volume, leads to an increase in the energy gain per particle and hence of the temperature. Note that, as expected, the molecular to atomic abundance ratio varies by a large factor over the range of A_{v0} values, from $[H_2]/[H]$=0.1 for $A_{v0} = 0.03$ mag to 40 for $A_{v0} = 1$ mag.

The ion-neutral drift velocity influences T_{max} due to heating through ion-neutral friction. Over the above range for v_D, T_{max} varies by 25% only. The density has a comparable influence (T_{max} decreases only by 20% as n_{H} increases from 20 to 100 cm^{-3}): the enhanced rate of radiative cooling as the density increases is counterbalanced by the longer crossing time (for the reason given above), providing the fluid particle with more time to heat up, and to a lesser extent by the decrease of the particle number density, as H_2 forms more efficiently on dust grains. The initial value of the ratio $n(H_2)/n(H)$ changes from 2.8 to 9.6 as n_{H} increases from 20 to 100 cm^{-3}. As $\Gamma_{d,max}$ is increased by a factor 10, T_{max} increases only by 10% because the crossing time is reduced (r_0 decreases by $\sqrt{10}$) and the time spent by the fluid cell in the layers of large shear is therefore significantly reduced. In summary, the gas temperature depends very weakly on the variations of the four parameters of importance, over the range of their plausible values.

In addition to their influence on the temperature, these parameters have more direct effects, such as the decrease of photodissociation rates as A_{v0} increases, or the increase of the binary reaction rates with the density. The interplay of all the previous effects upon the column density of molecules formed in the vortex is illustrated in Fig. 3. It displays the dependence of the OH, CH^+, H_2O and HCO^+ column densities integrated across the vortex on these four parameters.

All the species but CH^+ have column densities integrated across the vortex filament which steadily increase with A_{v0}, the extinction at the location of the burst. CH^+ is not only formed but also destroyed in reactions with H_2, and its abundance eventually falls off as A_{v0} rises. The dependences on $\Gamma_{d,max}$ and v_D are complex to interpret because the radius of the vortex r_0 has to be adjusted in each case to allow one parameter only to vary, as explained above. The column density which is proportional to r_0 is therefore a combination of the variations of the fractional abundances and of the vortex radius. Nonetheless, it is striking that all species but CH^+ have the same dependences on all the parameters, despite their different formation routes.

The ratios of column densities of different molecules are significant predictions of the model which can be easily compared to observations. Fig. 4 displays the dependence of three ratios $N(OH)/N(HCO^+)$, $N(OH)/N(CH^+)$ and $N(CH)/N(CH^+)$ on the same parameters. The most remarkable result is the small relative variation of the ratio $N(OH)/N(HCO^+)$ as A_{v0} varies between 0.1 and 1 mag. At first sight, this is surprising, since the chemical processes which

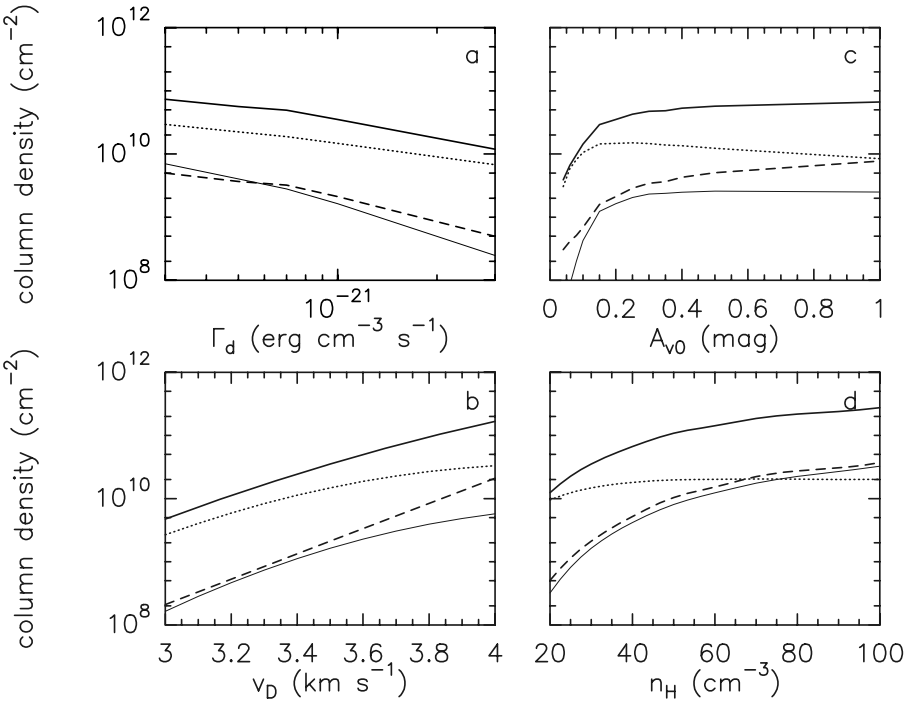

Fig. 3a–d. Dependence of the column densities across the vortex of four species, OH (thick solid line), CH^+ (dotted line), HCO^+ (thin solid line) and H_2O(dashed line) on: **a** the viscous heating rate, **b** the ion-neutral drift velocity, **c** the visual extinction and **d** the total proton density.

form OH and HCO^+ are independent. However, it turns out that the column densities of both species have only a weak dependence on A_{v0} (see Fig. 3c). In comparison, the ratios $N(CH)/N(CH^+)$ and $N(OH)/N(CH^+)$ increase with A_{v0} by a much larger factor (Figs. 4b and c): the column density of CH and OH depend only weakly on the UV shielding for $A_{v0} > 0.2$ mag, whereas that of CH^+ decreases with increasing A_{v0}. The ion-neutral drift velocity has much less influence on these ratios than it has on the column densities (see Fig. 3b). As expected from the influence of the density upon the column densities (Fig. 3d), the two abundance ratios involving CH^+ are significantly sensitive to n_H, more than the $N(OH)/N(HCO^+)$ ratio.

4. Comparison with the observations

It has been known for a long time that OH emission is not correlated with CO emission and that the OH abundance peaks towards the (more atomic) edges of molecular clouds (Wannier et al. 1993). More recently, molecular observations in absorption at mm-vawelengths have revealed an unexpected richness in molecules of a gaseous component which is only weakly shielded from the ambient ISRF (Lucas & Liszt 1993, 1994, 1996; Liszt & Lucas 1993, 1995, 1996; Hogerheijde et al. 1995). The fractional abundances of molecular species such as HCO^+ and OH are found to exceed by two orders of magnitude the values predicted by static diffuse cloud chemistries. The column density of OH detected in absorption reaches values, relative to atomic hydrogen, as large as N(OH)/N(H)$= 1.2 \times 10^{-6}$ (Lequeux, private communication), whereas the values predicted by gas-phase chemical models of diffuse clouds are of the order of 10^{-8}. Neither can the large observed abundances of HCO^+ be reproduced by current chemical schemes in diffuse gas (Lucas & Liszt 1996).

A few clues are provided by the set of observations quoted above. The column densities of OH and HCO^+ detected in absorption have been found by Lucas & Liszt (1996) to be closely correlated. The OH and HCO^+ absorption lines are found to have similar centroid velocities and widths. There is no obvious correlation between the CO emission or absorption components and those detected in OH and HCO^+ (Liszt & Lucas 1996).

4.1. The observed column densities

The observational data that we have used for comparison with our model are either sets of CH, CH^+ and OH absorption lines observed in the visible range in the direction of nearby stars (Crutcher & Watson 1976; Federman et al. 1996b; Felenbok & Roueff 1996 and references therein; Crane et al. 1995) and Southern OB stellar associations (Gredel 1997), or OH and HCO^+ absorption lines observed at mm-wavelengths against extragalactic continuum sources (Lucas & Liszt 1996; Liszt & Lucas 1996) for which H I absorption measurements also exist. The total gas column densities along the lines of sight are determined from the color excess of the star or the extinction to the association in the visible. In the radio domain, only the column density of atomic hydrogen is known from the H I lines, that of H_2 not being measurable directly for these lines of sight.

In the CH and CH^+ data sets, there is an indication that the observed column densities of these molecules increase with the total gas column density along the line of sight, although the scatter of the data points is large. We have merged the samples of Crane et al. (1995) for which the stars cover the extinction range $0.03\,\mathrm{mag} < A_v < 1.5\,\mathrm{mag}$ and that of Gredel (1997), with a

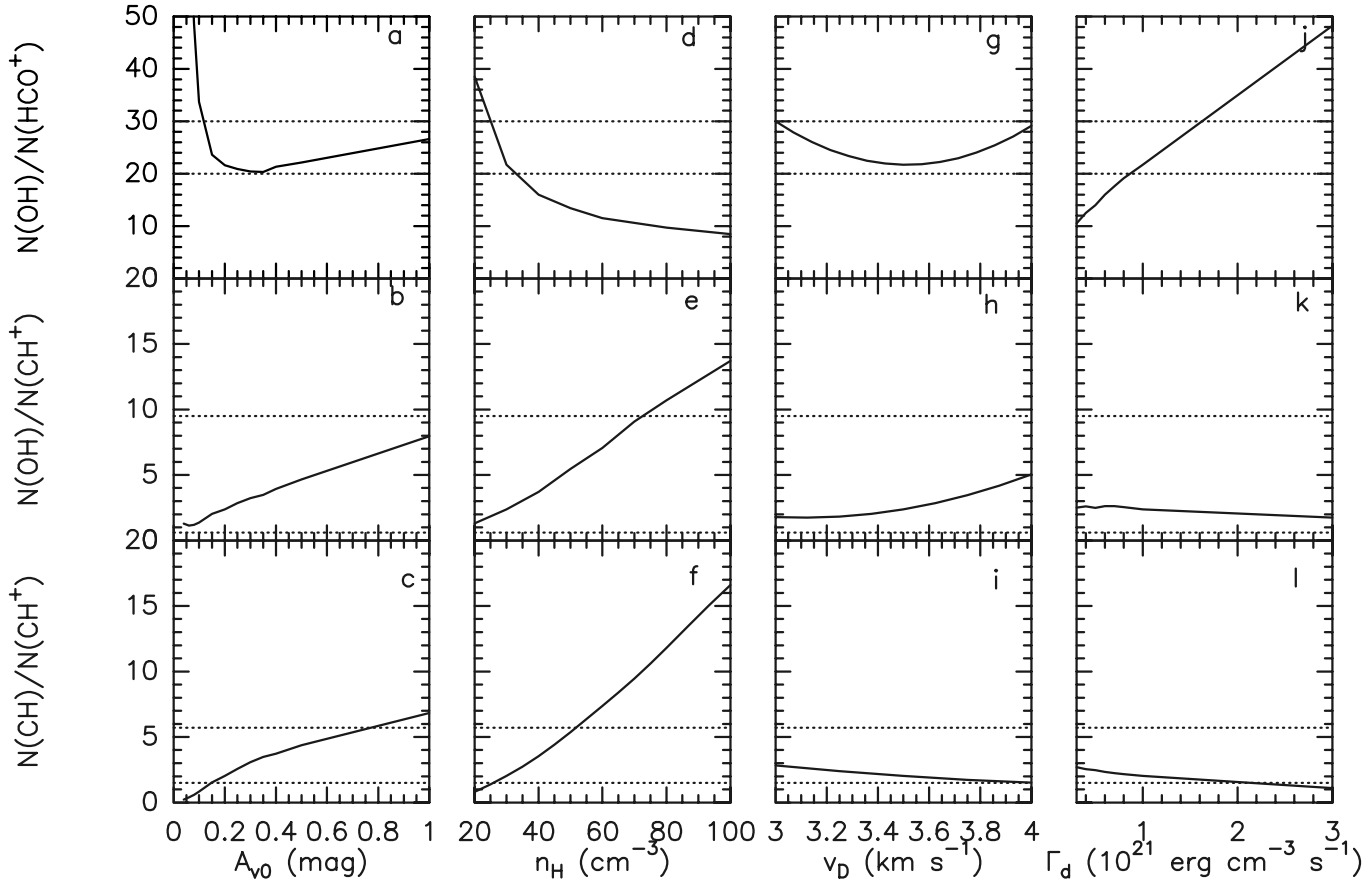

Fig. 4a–l. Dependence of the ratios $N(\mathrm{OH})/N(\mathrm{HCO}^+)$, $N(\mathrm{OH})/N(\mathrm{CH}^+)$ and $N(\mathrm{CH})/N(\mathrm{CH}^+)$ of the column densities integrated across the vortex on the UV shielding (**a** to **c**), the total cloud density (**d** to **f**), the ion-neutral drift velocity (**g** to **i**) and the viscous dissipation rate (**j** to **l**). The dotted lines in each panel delineate the range of observed values (see references in Sect. 4.1).

larger range in A_v ($0.5\,\mathrm{mag} < A_v < 4.5$ mag), and find that the column densities of CH^+ and CH increase similarly with the total column density along the line of sight i.e. $N(\mathrm{CH})/N_\mathrm{H} \approx 2.5 \times 10^{13}$ cm^{-2} mag^{-1} and $N(\mathrm{CH}^+)/N_\mathrm{H} \approx 1.5 \times 10^{13}$ cm^{-2} mag^{-1} with a scatter of a factor 2 in each direction. The OH lines in the direction of the four stars where they have been detected provide N(OH)$\approx 6 \times 10^{13}\,\mathrm{cm}^{-2}$ per magnitude.

The above column densities per magnitude enable us to estimate the number of standard dissipative structures per magnitude intercepted by a random line of sight across the diffuse medium, (assuming for the sake of simplicity that all the vortices have their axis perpendicular to the line of sight). Considering the column densities integrated across 10^3 individual vortices given in Table 1, the average number of vortices per magnitude is about 10^3 for CH^+ and CH and 1.7×10^3 for OH. The scatter of the observed values in the sample of Gredel and Crane et al. allows this number to range between ≈ 500 and 2×10^3 structures per magnitude.

The column density of CO corresponding to 10^3 structures on a line of sight is $N(\mathrm{CO}) \approx 3 \times 10^{12}$ cm^{-2} which is too small to be detected in the radio domain in absorption (see recent results from Lucas & Liszt 1997) or in emission; this explains why in most cases CO is not seen on those lines of sight where HCO^+ and OH are detected. The total CO column density relative to hydrogen, $N(\mathrm{CO})/N_\mathrm{H} = 5.6 \times 10^{-9}$ is comparable to the smallest values observed in the UV range in absorption against nearby stars (Federman al. 1980).

The column densities reported in Table 1 allow a comparison of the respective contributions of the vortices and the ambient medium to the total values. For all the species but CO and $\mathrm{H_2O}$ the contribution of the ambient medium is smaller than that of the vortices, and in a few cases completely negligible. There is about twice as much neutral carbon in the vortices than in the ambient medium and the total column density of neutral carbon relative to hydrogen is $N(\mathrm{C})/N_\mathrm{H} = 1.1 \times 10^{-7}$ for 1000 vortices per magnitude. It falls within the range of values $2 \times 10^{-8} < N(\mathrm{C})/N_\mathrm{H} < 2 \times 10^{-6}$ deduced from the observations of Jenkins & Shaya (1979). Hence, a non negligible fraction of the neutral carbon detected in the diffuse medium is likely to be produced in the dissipative structures of turbulence.

We cannot derive a number of dissipative structures *per magnitude* of gas from the observations at mm-wavelengths because the fraction of $\mathrm{H_2}$ along the lines of sight is unknown. A comparison of the model predictions with the data of Lucas & Liszt (1996) is shown in Fig. 5 for 10^3 and 3×10^3 *standard* structures on the line of sight and a whole range of values of the visual

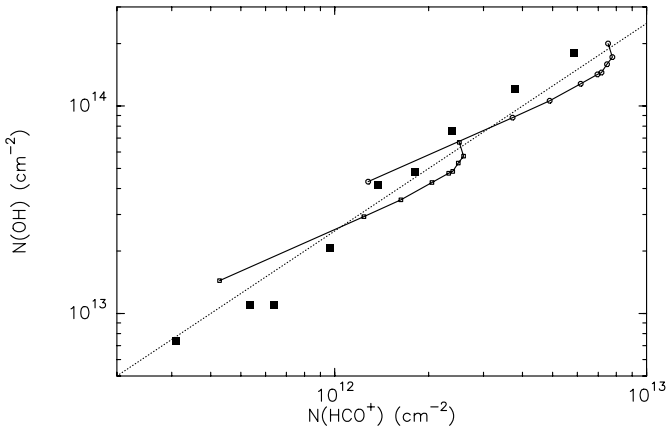

Fig. 5. The correlation between the column densities of OH and HCO^+. The observations of Lucas & Liszt (1996) are shown (solid squares). The error bars are smaller than the size of the symbols. The dotted line displays $N(OH)/N(HCO^+) = 25$. The column densities predicted by the model are given by the two curves, for two cases: 10^3 and 3×10^3 standard vortices on the line of sight. Each point along these curves corresponds to a different value of A_{v0} from 0.1 mag to 1 mag.

extinction from $A_{v0} = 0.1$ to 1 mag. It is gratifying that the values predicted for N(OH) and $N(HCO^+)$ all fall within the small scatter of the data points. Note that the column densities of OH are those derived from the absorption features only. We show in Sect. 4.3 that the OH molecules in the ambient medium do not contribute to the absorption features. The OH absorption lines in the radio domain therefore sample only the dissipative structures. The same is true for HCO^+ but for a different reason: the production of HCO^+ in the ambient medium is negligible (see Table 1).

These results suggest that observations in the visible range, in absorption against stars, and in the radio range, in absorption against extragalactic continuum sources, sample comparable column densities of diffuse gas, with similar non-equilibrium chemical properties.

For a total density $n_{\rm H} = 30\,{\rm cm}^{-3}$, the pathlength corresponding to 1 mag (or $N_{\rm H} = 1.8 \times 10^{21}$ cm^{-2}) is 20 pc. It is then possible to compute the fraction of hot gas along a line of sight required to reproduce the observed column densities. Estimating that each vortex has a hot layer of thickness $\approx 2r_0$ (see Fig. 1), we find $2 \times 10^{-3} < N_{hot}/N_{\rm H} < 8 \times 10^{-3}$ for a range of 500 to 2000 in the number of vortices per magnitude. Hence, *less than one percent* of hot gas on any line of sight is therefore needed to reproduce the observed properties of CH^+, CH, OH and HCO^+ in diffuse clouds.

4.2. Constraints provided by the observed column density ratios

The values of the observed column densities provide an estimate of the number of active dissipative structures along a line of sight at any time. The ratios of these column densities and their degree of scatter put constraints on the parameters discussed in the previous section. In the analysis below, we have neglected the contributions due to the ambient medium for CH, CH^+ and HCO^+ and for OH observed in the radio domain as explained in the next section. But the ambient medium contributes 37% of the OH absorption in the visible range (see Table 1).

One of the most striking features of the observational results is the small variation of the ratio $N(OH)/N(HCO^+) = 25 \pm 5$ over a range of about 30 in column densities (see Fig. 5). The $N(CH)/N(CH^+)$ ratio is also rather well defined although the scatter of observed values is much larger than for OH and HCO^+. From the sample of Crane et al. (1995), we derive $N(CH)/N(CH^+) \approx 1.5$. Gredel (1997) finds a linear correlation between $N(CH)$ and $N(CH^+)$ with slopes about 2 depending on the sample. The largest values of $N(CH)/N(CH^+) = 5.7$ and 4 are reported in Felenbok & Roueff (1997) in front of the stars ζ Per and HD 27778 from the observations of Jura & Meyer (1985), Federman et al. (1994), Federman (1982) and Meyer & Roth (1991). On the other hand, the $N(OH)/N(CH^+)$ ratio varies significantly. OH lines have been detected in the visible range in front of 4 nearby stars, ζ Per, HD 27778, o Per and ζ Oph (Crutcher & Watson 1976; Federman et al. 1996b; Felenbok & Roueff 1997). The ratio $N(OH)/N(CH^+)$ varies from 1 to 15 but the statistical significance of the sample is low. The contribution of the ambient medium to this ratio must be removed to compare the data to the model predictions. For the above estimate of 37%, the range of observed OH/CH^+ ratios to be compared to the model predictions is reduced to 0.6-9.5, since the ambient medium does not contribute to the CH^+ column density. The ranges of observed values of OH/HCO^+, OH/CH^+ and CH/CH^+ are displayed in Fig. 4 as dotted lines.

It is noteworthy that all the data sets provide the same constraints (or the same lack of constraint) on the parameters discussed in Sect. 3. Any value of A_{v0} between 0.1 and 0.8 mag is consistent with the observed ratios (Figs. 4a to c). This means that wherever the burst of dissipation occurs in a diffuse cloud, the OH/HCO^+, OH/CH^+ and CH/CH^+ abundance ratios will be in the range of those observed. Analogous statements apply to the ion-neutral drift velocity, the values of which have been dictated by the observed characteristic of the turbulence in diffuse gas. On the other hand, the computed ratios depend on the cloud density and the comparison with the observed values (Figs. 4d to 4f) suggests that the hot chemistry has to develop in low density gas $n_{\rm H} \lesssim 70$ cm^{-3} characteristic of diffuse clouds. Lastly, the dependence on the viscous dissipation rate (Figs. 4j to l) suggests that dissipation rates close to that of the standard model are consistent with the data.

In summary, the observations support the proposal that the hot chemistry is triggered by dissipative bursts of average strength anywhere in a diffuse cloud, i.e. a cloud of low density, poorly shielded from the ISRF, and with a turbulent rms velocity dispersion of 3 to 4 km s^{-1}.

4.3. OH emission and absorption

The OH observations of Liszt & Lucas (1996) show that, contrary to H I observations, the gas visible in OH absorption is

not always seen in emission above their detection limit (rms $\sigma \approx 0.01$ K) and that the OH emission in most cases has a much broader velocity coverage ($\Delta v_{em} \approx 10$ km s^{-1}) than do the OH absorption features ($\Delta v_{abs} \approx 1$ to 2 km s^{-1}). The velocity coverage of the OH emission agrees quite well with that of the H I absorption components. Liszt & Lucas propose that pockets of gas rich in OH are widely distributed within the atomic gas but at sufficiently small scale that not all the lines of sight intercept these pockets at all the H I velocities. We suggest here that the OH emission arises mainly in the bulk of the diffuse cloud responsible for the H I absorption lines, while the OH absorption originates in the OH-rich component generated by the dissipative structures. We discuss below the various constraints on the characteristics of the structures (spatial distribution, optical depth) provided by the emission and absorption data of Liszt & Lucas.

We first derive an estimate of their beam filling factor from the comparison of the OH emission and absorption at the velocity of the absorption features. In the Rayleigh-Jeans approximation, the intensity of the OH line in emission is given by:

$$T_{em} = f_s(1 - \mathrm{e}^{-\tau})(T_{ex} - T_{BG}) \tag{22}$$

where T_{ex} is the excitation temperature of the OH molecules, T_{BG} is the temperature of the Cosmic Background, τ the optical depth of the line at the line centroid velocity and f_s the beam filling factor of the emitting gas. The observations reported by Liszt & Lucas reveal that the intensity of the line emission T_{em} at the velocity of the absorption features tends to increase with the optical depth of the OH absorption as $0.5\mathrm{K} < T_{em}/\tau < 2\mathrm{K}$ over the range of measured opacities in absorption, $0.01 < \tau < 0.2$. The OH excitation temperature in the dissipative structures is estimated following Guibert et al. (1978):

$$T_{ex} = T_k \frac{T_{BG} + T_0}{T_k + T_0} \tag{23}$$

with $T_0 = 7 \times 10^{-3}[n(\mathrm{H}) + n(\mathrm{H_2})]\sqrt{T_k}$. The kinetic temperature has been computed by following the isobaric cooling of the gas chemically enriched, after the turn-off of the viscous intermittent heating. We have found that the OH enrichment over the ambient gas is maintained over $t \approx 10^3$ yr, while the kinetic temperature has already dropped to $T_k = 450$ K. This result is similar to that presented in FPR. We therefore adopt the range $450\mathrm{K} < T_k < 10^3\mathrm{K}$ for the kinetic temperature of the OH-rich gas. The density of collisional partners is $n(\mathrm{H}) + n(\mathrm{H_2}) = 16.6$ cm^{-3} in the case of the standard model and we find $T_{ex} = 6.3$ K and 5.1 K for $T_k = 10^3$ K and 450 K respectively. We therefore deduce from Eq. (22) that the beam filling factor of the large number of structures responsible for an absorption feature has to be smaller than unity in emission, $0.3 < f_s < 0.4$ for the average value $T_{em}/\tau \approx 1$ K. The possible range of values for f_s extends from 0.15 up to 0.8 when the whole range of values of T_{em}/τ is considered. These filling factors are not small, which explains why the probability of detecting an OH absorption feature with τ in the range 0.01 - 0.2 on a random line of sight is also not small, the probability being larger for smaller optical depth components. This is indeed the shape of the probability distribution of $\mathrm{HCO^+}$ optical depths found by Lucas & Liszt (1996, see their Fig. 4). In what follows, we adopt $f_s \approx 0.5$ which means that an important fraction of lines of sight toward extragalactic sources (half, on average) should intercept a number of dissipative structures large enough to be detected in absorption.

The OH optical depth of the main radio components being given by:

$$\tau = 4.5 \times 10^{-15} N(\mathrm{OH})/T_{ex}\Delta v, \tag{24}$$

where Δv the linewidth is expressed in km s^{-1}, we calculate the OH column density responsible for an absorption feature ($\Delta v_{abs} \approx 1$ km s^{-1}) to be $N(\mathrm{OH}) = 1.4 \times 10^{13}(\tau/0.01)$ cm^{-2} for $T_k = 10^3$ K; it is only 1.2 times smaller for $T_k = 450$ K. Such OH column densities correspond to ≈ 300 up to 8×10^3 standard structures on the lines of sight.

In addition to the gas detected in OH absorption which fills only a fraction of the velocity coverage of the H I absorption lines, the spectra of Liszt & Lucas reveal a component seen in OH emission only, which approximately covers the whole velocity range of the H I absorption lines. We argue below that this emission may arise in the bulk of the ambient medium, because the OH optical depth of this medium is likely to be smaller than that of OH in the dissipative structures. The column densities of OH in the dissipative structures and in the ambient gas are of the same order of magnitude (see Table 1). The excitation temperatures are not significantly different ($T_{ex} = 4$ K for the ambient gas at $T_k = 100$ K instead of $T_{ex} = 6.3$ to 5.1 K for the structures) but the velocity range over which the ambient gas is distributed is much larger ($\Delta v \approx 10\,\mathrm{km\,s^{-1}}$) than for the individual absorption features ($\Delta v \approx 2$ km s^{-1}). It is this difference in the velocity distribution which makes the optical depth of the ambient gas smaller than in the structures, preventing its detection in absorption in the present data set. It is seen in emission, at a level slightly smaller than the gas detected also in absorption, because its beam filling factor is not smaller than unity.

4.4. Line widths and line centroids

There appears to be no systematic difference in the line centroid velocities of CH and $\mathrm{CH^+}$ seen in absorption in front of a number of sources (Gredel 1997; Crane et al. 1995; Crawford 1995). The same is true for the OH and $\mathrm{HCO^+}$ line centroids (Lucas, private communication). Histograms of the $\mathrm{CH^+}$ and CH line widths show that the $\mathrm{CH^+}$ lines are on average 1.5 to 2 times broader than the CH lines, with linewidths of the order of 4 km s^{-1} on average (Crane et al. 1995; Crawford 1995). The line widths of the OH and $\mathrm{HCO^+}$ absorption lines are similar and close to 2 km s^{-1} (Lucas, private communication).

At first sight, the observed similarity of the OH and $\mathrm{HCO^+}$ linewidths and, even more, the larger line widths of $\mathrm{CH^+}$ compared to those of CH, seem to contradict the scenario proposed, in which the neutrals partake in the velocity field of the vortex while ions are held by the magnetic field lines. This conflict has its origin in the fact that, for the sake of simplicity, we have

assumed that the ions, owing to their interaction with the magnetic field, have zero velocity and that the large ion-neutral drift arises solely from the motion of the neutral gas in the vortex. In addition, the vortex filaments are assumed to be straight, which is also a crude simplification of the reality in which vortex filaments probably spiral around one another and form braided structures (see Porter et al. 1994). In the interstellar medium, magnetic field lines are set into motion by Alfvén waves and a self-consistent treatment of the problem would require a description of the environment of the vortices up to the larger scales of turbulence which act upon the magnetic field lines. This is far beyond the scope of the present work. It is even beyond the capabilities of the present numerical simulations, which cannot properly describe the microscopic physics at the scales close to those of viscous dissipation. The differences between the CH^+ and HCO^+ linewidths are not explained either by the present model.

4.5. Rotational H_2 *line intensities*

We have computed the intensity (integrated over the linewidth) of the H_2 pure rotational transitions emitted by a standard structure,

$$I_{ul}(\mathrm{H_2}) = \frac{1}{4\pi}(4J_u - 2)BN_uA_{ul} \tag{25}$$

where $B = 1.17 \times 10^{-14}$ erg is the rotational constant. The results are given in Table 2 for an ensemble of 10^3 vortices intercepted by a line of sight (i.e. sampling 1 mag of diffuse gas). For comparison, the H_2 line emission of the ambient gas on the same line of sight is also given for an ortho/para ratio of unity. The results are barely different for an ortho/para ratio of 3. The $[H_2]$/[H] ratio in the ambient medium is supposed to be unity as in Sect. 3.3.

The comparison of the emission in the two lowest rotational lines from the vortices and from the ambient medium clearly shows that the vortices radiate the bulk of their energy in the S(1) and S(2) lines, while the ambient medium does so in the S(0) line. Furthermore, the ensemble of 10^3 vortices, filling only 1% of the line of sight, radiate almost ten times more energy in the H_2 lines than the ambient medium which fills 99%. Observations with the SWS aboard the ISO satellite have been performed to determine the spectrum of the rotational H_2 emission in the diffuse medium of the Galaxy. They will be presented in a forthcoming paper (Verstraete et al., in preparation).

It is also interesting to note that the S(1) line emission from the dissipative structures is almost as intense as the radiation emitted in the C II line at 158 μm by the ambient medium. For a line of sight crossing 1 mag of the diffuse medium, the C II line emission would be I(158 μm)= 3.8 $\times 10^{-6}$ erg cm^{-2} s^{-1} sr^{-1}, deduced from the average computed cooling rate $\Lambda(158\,\mu\mathrm{m}) \approx 8 \times 10^{-25}$ erg cm^{-3} s^{-1}. But unlike that of the S(1) line, the C II emission from the dissipative structures is negligible (less than 1%) compared to the emission arising in the ambient gas.

5. Energy balance

It is essential to check that the energy required in the model proposed above to account for the column densities of molecules observed in diffuse clouds does not exceed the amount of turbulent kinetic energy available in the cascade. Diffuse clouds are connected to their galactic environment and receive turbulent energy from it. As discussed in FP, the average rate of kinetic energy transfer to diffuse clouds, deduced from observations, is $\epsilon = 0.014$ erg g^{-1} s^{-1}; this is a geometric average, the plausible range extending from 10^{-3} to 0.2 (in the same units). These numbers are deduced from the high latitude H I data in the Leiden/Dwingeloo survey (Hartmann & Burton 1997).

We estimate now the amount of energy required to feed a 'hot chemistry' such as that observed in diffuse clouds. We assume that, at any time, a large number of structures similar to those described in Sect. 2 are dissipating energy along any line of sight, each at a rate $\Gamma_d = 10^{-21}$ erg cm^{-3}s^{-1}. The heating rate due to the ion-neutral friction is 20 times smaller than Γ_d in the standard model and corresponds to only 10% of the viscous dissipation once integrated over the active fraction of the cloud volume; it is therefore neglected in the following. The active fraction of the gas is at most $A \approx 10^{-2}$ on a line of sight, but most likely f_sA since, as discussed in Sect. 4.3, the beam filling factor of active structures at any time is likely to be smaller than unity. The same fraction f_sA of the cloud volume $\mathcal{V}$ (or of its mass M, since the density is assumed uniform) is therefore on average affected by the intermittent dissipation at any time. The energy dissipation rate is therefore $\epsilon_d = f_s\,A\,\Gamma_d\,\mathcal{V}/M = f_s\,A\,\Gamma_d/\rho$ where $\rho = 7 \times 10^{-23}$ g cm^{-3} is the gas density of the standard model. The total amount of turbulent energy dissipated per unit time and mass is therefore

$$\epsilon_d = 7 \times 10^{-2} \left(\frac{f_s}{0.5}\right) \text{erg g}^{-1}\ \text{s}^{-1}. \tag{26}$$

Although they fill only a tiny fraction of the volume, coherent vortices in laboratory flows account for 10% to $\approx$ 30% of the total viscous dissipation; this percentage might even be larger at higher Reynolds numbers (Jimenez 1997). The total dissipation rate in diffuse clouds is therefore likely to be up to a few times the above value. This estimate is only crude, but it is interesting that the result is somewhat smaller than the upper values of the energy transfer rate inferred from H I observations. Therefore, on average over a $\approx$ 10 pc scale, the amount of energy required to reproduce the observed signatures of 'hot chemistry' in the diffuse gas does not exceed the amount of energy available in large scale turbulence. This dissipation rate may be compared to the kinetic energy transfer rate in the least virialized molecular clouds, i.e. those for which the internal kinetic energy is large compared with their gravitational potential energy (Falgarone, Puget & Pérault 1992). The observed scaling laws between the internal velocity dispersion and the size of such clouds provide the estimate $\epsilon \approx 10^{-3}$ erg g^{-1} s^{-1} at the parsec scale. One might speculate that a non-negligible fraction of the turbulent energy content of a diffuse cloud is being permanently dissipated, through elastic collisions and ion-neutral drag, in the

Table 2. Predicted intensities of the lowest rotational transitions of H_2 for standard dissipative structures.

Line	λ (μm)	$J_u - J_l$	E_u/k (K)	A_{ul} (s^{-1})	$I_{ul}(H_2) \times 10^3$ (1 mag) (erg cm^{-2} s^{-1} sr^{-1})	Ambient gas (1 mag) (erg cm^{-2} s^{-1} sr^{-1})
S(0)	28.2	2-0	170	2.95×10^{-11}	3.4×10^{-7}	3.5×10^{-7}
S(1)	17.03	3-1	510	4.77×10^{-10}	1.6×10^{-6}	5.1×10^{-9}
S(2)	12.28	4-2	1020	2.76×10^{-9}	8.9×10^{-7}	4.8×10^{-13}
S(3)	9.66	5-3	1700	9.86×10^{-9}	1.3×10^{-7}	
S(4)	8.03	6-4	2540	2.65×10^{-8}	4.7×10^{-9}	

intermittent structures which are unevenly scattered throughout the cloud volume. This energy dissipation creates not only radiation, but also a whole set of molecular species, as seen above. That small fraction of the turbulent energy which is not dissipated in diffuse clouds could be transferred to the molecular clouds which are immersed in the diffuse medium, and be the source of their suprathermal motions before it eventually dissipates there.

6. Discussion: effects of repeated impulsive heatings

The above comparison with observational results suggests that the essential features of the model are correct, namely, the close association in space and time of the regions where the 'hot chemistry' occurs, owing to the large ion-neutral drift and the enhanced kinetic temperature. The model ensures the similarity of the line centroids of the various species and the observed proportionality of the abundances of HCO^+ and OH, in spite of their very different formation routes. It also explains why the gas rich in OH, which is so closely related to the HCO^+ rich component, is not seen systematically in emission.

Nonetheless, the lifetime of the coherent vortex filaments that we have chosen as templates for the dissipative structures might be smaller than the timescales in which the 'hot' chemistry is active. The main reason is that the gas in the vortex is not prevented from expanding under the combined actions of the thermal pressure gradient and centrifugal force. For the parameters of the standard model, the gas acceleration resulting from this imbalance causes the vortex to double its radius within the vortex period $P = 23$ yr. In our model, the crossing time of the active layers, $\tau_c \approx 100$ to 200 yr, is larger than the vortex period, and the vortex is assumed to survive over about 8 periods. We have no experimental or theoretical means of estimating the actual lifetime of such vortices, nor their confinement. We have therefore considered the possibility that the 'hot' chemistry is activated over short timescales, but a large number of times in the same fluid cell. We show below that, because of the large thermal and chemical inertia of the gas, the signature of the hot chemistry disappears only slowly (see also FPR), and that column densities comparable to those obtained within the approximately 200 yr spent in a single vortex may be obtained after much shorter but repeated incursions into a few vortices bunched together.

Instead of activating the hot chemistry once only within a supposedly long-lived vortex, it is activated at each encounter with a new short-lived vortex. We have investigated the impact upon the chemistry of a cell which is trapped in a vortex for about one period only and then, after some time spent in the inactive part of the cloud, enters another nearby vortex, and so on. We have assumed that chemical activity is triggered when the cell enters the layers of large ion-neutral drift and large viscous dissipation rate. The succession of trappings in vortices is introduced in the cell time-dependent evolution as a set of Gaussian increases in Γ_d and in ion-neutral drift velocity, occurring at regular intervals.

The time-dependent evolution of the temperature is displayed in Fig. 6a for two periods of the successive trappings, 260 yr and 130 yr. In both cases, the time during which the ion-neutral drift velocity exceeds 3 km s^{-1} is only 26 yr, comparable to the vortex period, and that when the viscous heating rate exceeds 5×10^{-22} erg cm^{-3}s^{-1} is 23 yr. The ratio of these timescales has been chosen to be the same as in the standard model. The fractional abundances of OH, CH^+, H_2O and HCO^+ are shown in Fig. 6b for the long period case and the same parameters as the standard model to describe the vortex.

It is noteworthy that the large thermal inertia of the gas allows the temperature to rise steadily, on average, up to a regime where it oscillates about constant values. Efficient H_2 cooling prevents the maximum temperature from being quite as large as in the standard model (see Fig. 1), but the difference is small. Even for the case of long inactivity (260 yr) between encounters with a vortex, the kinetic temperature continues oscillating between 800 K and 950 K after only six encounters. Fig. 6b also shows that less than six interactions with short-lived vortices are sufficient to enrich the gas and produce abundances close to those obtained after crossing one standard long-lived vortex (see Fig. 2). The times required to reach the maximum abundances are comparable in both descriptions, the long and short-lived vortices. The chemical inertia is large for OH and H_2O as suggested by the small amplitudes of the abundance variations of these species. On the other hand, CH^+ disappears rapidly when its formation ceases to be driven by the large ion-neutral drift; to a lesser extent, the same is true for HCO^+.

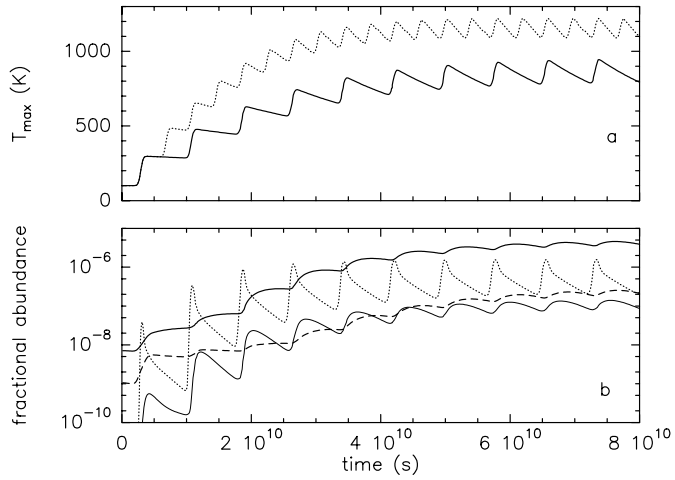

Fig. 6a and b. Thermal and chemical evolution of a cell periodically trapped in standard vortices. **a** The time-dependent evolution of the temperature. The time between each active period is 260 yr (solid lines) and 130 yr (dashed lines), while the duration of the large ion-neutral drift and large viscous heating rate regimes are 26 yr and 23 yr respectively. Note the slow decrease of the temperature between each active period for $T_{\rm k} < 800$ K. **b** The time-dependent evolution of OH (thick solid line), CH^+ (dotted line), H_2O (dashed line) and HCO^+ (thin solid line) fractional abundances for a period of activity of 260 yr. After only a few encounters, the fractional abundances continue oscillating around values close to those obtained in the standard model (see Fig. 2).

7. Conclusions

The model that we have proposed here to describe the intermittent dissipative structures of turbulence and their impact upon the chemistry of the diffuse gas is clearly an idealization, but it allows a quantitative prediction of the influence of two physical processes: the viscous dissipation and the large ion-neutral drift velocities. These two processes are closely associated in space and time, and the energies involved enable us to reproduce, without fine-tuning the parameters of the model, the salient features of the observations: *(i)* the large column densities of CH^+, OH and HCO^+ in diffuse clouds, *(ii)* the proportionality of the OH and HCO^+ column densities, *(iii)* the similarity of the OH and HCO^+ line centroids, and those of the CH and CH^+ lines, and *(iv)* the fact that the OH-rich gas seen in absorption is not always detected in emission.

A major result is that less than one percent of the gas on a line of sight trapped at any time in these coherent structures is sufficient to reproduce the large column densities of OH, CH^+ and HCO^+ observed in the diffuse medium. Thus, average physical properties, deduced from the observations, are not necessarily relevant to the description of the evolution of the gas when the fluctuations are large. We have proposed that the principal contributions to the column densities of OH, CH^+ and HCO^+ arise within the 1% or so of a line of sight where the kinetic temperature is about ten times its average value. The estimated number of dissipative structures along a line of sight of total column density corresponding to 1 mag of visual extinction is about 10^3 on average at any given time. The amount of turbulent energy dissipated on average in all these structures within a large scale diffuse cloud, which is the energy source of the 'hot' chemistry, is smaller than the kinetic energy available in the turbulent cascade in the diffuse medium.

Our model has difficulties in explaining the similarity of the ion and neutral linewidths; this problem originates in the idealized description of the magnetic field. We have assumed that the magnetic field lines, and the ions, are fixed whilst the neutrals partake of the motion of the vortex. A more realistic treatment should consider the effects of Alfvén waves on the field lines, as well as the large scale motions which probably contribute to the confinement of the small scale vortices. Such a treatment would involve a large range of scales, connected dynamically, and is beyond the scope of the present study. Moreover, the description of the dissipative structures of turbulence as coherent vortices is likely to be too restrictive (Jimenez, 1997). A multifractal description of the subset of space in which dissipation is concentrated may be more appropriate, as suggested by the power law distribution of observed optical depths, but no consensus has been reached yet on the validity of the two descriptions (coherent structures vs. multifractal) on the basis of laboratory flow experiments and numerical simulations.

The present work suggests that the cold diffuse medium may bear the signatures of a 'hot' chemistry triggered in localized regions of space which have the essential characteristics of Burgers vortices. The direct detection in emission of such vortices is beyond the capabilities of current telescopes. The existence of these coherent structures in the interstellar medium may be eventually inferred from other, indirect measurements, such as detections of the $J \geq 3$ pure rotational transitions of H_2 and of large abundances of H_2O, CH^+ and CH_3^+ in the cold neutral medium. If their existence is confirmed in the cold interstellar medium, it would imply that a significant fraction of the dissipation of supersonic interstellar turbulence occurs in regions of high vorticity similar to those currently observed in subsonic experiments at high Reynolds numbers, as opposed to shocks. These observations should be achievable with the next generation of space experiments, SIRTF and FIRST in particular.

Acknowledgements. We would like to thank Malcolm Walmsley for his critical reading of an early version of this paper which allowed us to significantly improve the manuscript, and Steve Federman for acting conscientiously as referee.

References

Abgrall H., Le Bourlot J., Pineau des Forêts G., et al., 1992, A&A 253, 525

Anders E., Grevesse N. 1989 Geochim. Cosmochim. Acta 53 197

Anselmet F., Gagne Y., Hopfinger E.J., Antonia R.A., 1984, JFM 140, 63

Bajer K., 1995, in *Small-scale structures in three-dimensional hydrodynamic and magnetohydrodynamic turbulence* eds. M. Meneguzzi et al. (Springer-Verlag: Berlin, Heidelberg)

Belin F., Maurer J., Tabeling P., Willaime H., 1996, J. Physique II 6, 573

Brandenburg A., Zweibel E.G., 1994, ApJ 427, L94
Brandenburg A., Procaccia I., Segel D., 1995, Phys. Plasmas 2, 1148
Brandenburg A., Jennings R.L., Nordlund A.K. et al., 1996, JFM 306, 325
Cadot O., Douady S., Couder Y., 1995, Phys. Fluids 7, 630
Crane P., Lambert D.L., Sheffer Y., 1995, ApJS 99, 107
Crawford I.A., 1995, MNRAS 277, 458
Crovisier J., 1981, A&A 94, 162
Crutcher R.M., Watson W.D., 1976, ApJL 203, L123
Douady S., Couder Y., Brachet M.E., 1991, PRL 67, 983
Draine B.T., 1980, ApJ 241, 1021
Falgarone E., Lis D.C., Phillips T.G., et al., 1994, ApJ 436, 728
Falgarone E., Pineau des Forêts G., Roueff E., 1995, A&A 300, 870
Falgarone E., Puget J.-L., Pérault M., 1992, A&A 257, 715
Falgarone E., Puget J.-L., 1995, A&A 293, 840
Federman S.R., Glassgold A.E., Jenkins E.B., Shaya E.J., 1980, ApJ 242, 545
Federman S.R., 1982, ApJ 257, 125
Federman S.R., Strom C.J., Lambert D.L., et al., 1994, ApJ 424, 772
Federman S.R., Rawlings J.M.C., Taylor S.D., Williams D.A., 1996a, MNRAS 279, 41
Federman S.R., Weber J., Lambert D.L., 1996b, ApJ 463, 181
Felenbok P., Roueff E., 1996, ApJ 465, L57
Flower D.R., Pineau des Forêts G., 1995, MNRAS 275, 1049
Flower D.R., Pineau des Forêts G., 1998, MNRAS 297, 1182
Flower D.R., Pineau des Forêts G., Hartquist T.W, 1985, MNRAS 216, 775
Flower D.R., Pineau des Forêts G., Hartquist T.W, 1986, MNRAS 218, 729
Gredel R., 1997, A&A 320, 929
Guibert J., Elitzur M., Nguyen-Q-Rieu, 1978, A&A 66, 395
Harding L.B., Guadagnini R., Schatz G.C., 1993, J. Phys. Chem. 97, 5472
Hartmann D.P., Burton W.B., 1997, *Atlas of galactic neutral hydrogen*, (Cambridge University Press)
Hogerheijde M.R., de Geus E.J., Spaans M., van Langevelde H.J., van Dischoeck E.F., 1995, ApJ 441, L93
Jenkins E.B., Shaya E.J., 1979, ApJ 231, 55
Jimenez J., 1997, in *Dynamics and statistics of concentrated vortices in turbulent flows*, Euromech Coll. 384
Jura M., Meyer D.M., 1985, ApJ 294, 238
Kay G.W.C., Laby T.H., 1966, *Tables of Physical and Chemical Constants* (London: Longmans)
Landau, L.D., Lifchitz E.M., 1959, *Fluid Mechanics* (Reading: Addison–Wesley)
Le Bourlot J., Pineau des Forêts G., Roueff E., Flower D.R., 1993, A&A 267, 233
Liszt H.S., Lucas R., 1994, ApJ 431, L131
Liszt H.S., Lucas R., 1995, A&A 294, 811
Liszt H.S., Lucas R., 1996, A&A 314, 917
Lucas R., Liszt H.S., 1993, A&A 276, L33
Lucas R., Liszt H.S., 1994, A&A 282, L5
Lucas R., Liszt H.S., 1996, A&A 307, 237
Lucas R., Liszt H.S., 1997: Molecules in Astrophysics: Probes and Processes, E.F. van Dischoeck (ed.), pp 421-430, Kluwer Acad. Pub.
Magnani L., Siskind L., 1990, ApJ 359, 355
Meneguzzi M., Pouquet A., 1981, J. Fluid Mech. 205, 297
Meyer D.M., Roth K.C., 1991, ApJ 413, L67
Moffat H.K., Kida S., Ohkitani K., 1994, JFM 259, 241
Myers P.C., Goodman A.A., Guesten R., Heiles C., 1995, ApJ 442, 177
Pérault M., 1987, PhD dissertation, Université Paris VII
Pineau des Forêts G., Flower D.R., Hartquist T.W., Dalgarno A., 1986, MNRAS 220, 801
Porter D.H., Pouquet A., Woodward P.R., 1994, Phys. Fluids 6, 2133
Savage B.D., Bohlin R.C., Drake J.F., Budich W., 1977, ApJ 216, 291
Schwarz K.W., 1990, PRL 64, 415
She Z.S., Jackson E., Orszag S.A., 1990, Nature 334, 226
Tabeling P., Zocchi G., Belin F., Maurer J., Willaime H., 1996, Phys. Rev E 53, 613
Vincent A., Meneguzzi M., 1991, JFM 225, 1
Vincent A., Meneguzzi M., 1994, JFM 258, 245
Wannier P.G., Andersson B.-G., Federman S.R., et al., 1993, ApJ 407, 163